HHS Public Access

Author manuscript

Cell Rep. Author manuscript; available in PMC 2022 June 22.

Published in final edited form as:

Cell Rep. 2021 March 30; 34(13): 108924. doi:10.1016/j.celrep.2021.108924.

Streptococcus pyogenes upregulates arginine catabolism to exert its pathogenesis on the skin surface

Yujiro Hirose[1,2,11,*],
Masaya Yamaguchi[1],
Tomoko Sumitomo[1],
Masanobu Nakata[3],
Tomoki Hanada[1],
Daisuke Okuzaki[4],
Daisuke Motooka[5],
Yasushi Mori[1],
Hiroshi Kawasaki[6,7,8],
Alison Coady[2],
Satoshi Uchiyama[2],
Masanobu Hiraoka[2,9],
Raymond H. Zurich[2],
Masayuki Amagai[6,8],
Victor Nizet[2,10],
Shigetada Kawabata[1,*]

[1]Department of Oral and Molecular Microbiology, Osaka University Graduate School of Dentistry, Suita, Osaka 565-0871, Japan

[2]Department of Pediatrics, University of California at San Diego School of Medicine, La Jolla, California 92093, USA

[3]Department of Oral Microbiology, Kagoshima University Graduate School of Medical and Dental Sciences, Kagoshima 890-8544, Japan

[4]Genome Information Research Center, Research Institute for Microbial Diseases, Osaka University, Suita, Osaka 565-0871, Japan

[5]Department of Infection Metagenomics, Research Institute for Microbial Diseases, Osaka University, Suita, Osaka 565-0871, Japan

[6]Department of Dermatology, Keio University School of Medicine, Tokyo 160-8582, Japan

[*]Correspondence: yujirohirose@dent.osaka-u.ac.jp (Y.H.), kawabata@dent.osaka-u.ac.jp (S.K.).

Author Contributions

Conceptualization, Y.H., M.Y., and S.K.; Methodology, Y.H., M.Y., T.S., M.N., Y.M, H.K., S.U., M.H., and M.A.; Software, D.O. and D.M.; Investigation, Y.H., A.C., and R.Z.; Formal analysis, Y.H. and T.H.; Data Curation, Y.H.; Supervision, M.Y., V.N., and S.K.; Visualization, T.H., D.O., and D.M.; Funding acquisition, Y.H., M.Y., V.N., and S.K.; Writing - Original Draft, Y.H.; Writing - Review & Editing, M.Y., T.S., M.N., V.N., and S.K.; Project administration, V.N. and S.K.

Declaration of Interests

The authors declare no conflict of interest.

[7]Immunology Data Integration Unit, RIKEN Medical Sciences Innovation Hub Program, Yokohama 230-0045, Japan

[8]Laboratory for Skin Homeostasis, RIKEN Center for Integrative Medical Sciences, Yokohama 230-0045, Japan

[9]Department of Otorhinolaryngology-Head and Neck Surgery, Wakayama Medical University, Wakayama, Wakayama 641-8509, Japan

[10]Skaggs School of Pharmaceutical Sciences, University of California at San Diego, La Jolla, California 92093, USA

[11]Lead contact

Summary

The arginine deiminase (ADI) pathway has been found in many kinds of bacteria, and functions to supplement energy production and provide protection against acid stress. The *Streptococcus pyogenes* ADI pathway is upregulated upon exposure to various environmental stresses, including glucose starvation. However, there are several unclear points about the advantages to the organism for upregulating arginine catabolism. We show that the ADI pathway contributes to bacterial viability and pathogenesis under low glucose conditions. *S. pyogenes* changes global gene expression, including upregulation of virulence genes, by catabolizing arginine. In a murine model of epicutaneous infection, *S. pyogenes* utilizes the ADI pathway to augment its pathogenicity by increasing the expression of virulence genes including those encoding the exotoxins. We also found that arginine from stratum corneum- derived filaggrin was a key substrate for the ADI pathway. In sum, arginine is a nutrient source that promotes the pathogenicity of *S. pyogenes* on the skin.

Introduction

One of the most important human bacterial pathogens of skin is *Streptococcus pyogenes*, which can produce superficial impetigo or more deep-seated cellulitis, but also more severe invasive infections such as sepsis, necrotizing fasciitis, and streptococcal toxic shock syndrome (Cunningham, 2000; Walker et al., 2014). *S. pyogenes* typing based on M protein and T antigen (pilus major subunit) antigenicity (Falugi et al., 2008) confirms several serotypes are capable of causing severe infections, but in recent decades one subclone of the M1 serotype, the globally disseminated clonal M1T1 clone (Chatellier et al., 2000), has persisted uninterruptedly as the most frequently isolated *S. pyogenes* strains from both invasive and noninvasive infections (Lynskey et al., 2019; Walker et al., 2014).

Human skin is an inhospitable environment that includes the physical barrier of the stratum corneum (SC), an acidic surface pH, and the active synthesis of innate defense factors such as antimicrobial peptides, proteases, lysozymes, cytokines, and chemokines that together serve to recruit immune cells and prime adaptive immune responses (Cogen et al., 2008; Proksch, 2018). To successfully colonize or establish infection in the skin, pathogens must possess virulence determinants for evasion of these immune factors and also for acquisition of nutrients, whose availability the host may restrict under the concept of nutritional

immunity. Elucidation of such bacterial metabolic pathways that are essential for *in vivo* survival can reveal unique targets for novel therapeutics.

The arginine deiminase (ADI) pathway is a metabolic pathway found in many kinds of bacteria that serves to supplement energy production and provide protection against acid stress *in vitro* (Abdelal, 1979; Cotter and Hill, 2003). The ADI pathway of *S. pyogenes* has been studied in a limited manner, and determined to antagonize nitric oxide (NO) production by macrophages and contribute to the asymptomatic colonization of the murine vaginal mucosa (Cusumano et al., 2014). The *S. pyogenes* ADI pathway is negatively regulated by three virulence-related transcriptional control systems: the control of virulence (CovRS) two-component gene regulatory system, catabolite control protein CcpA, and regulator gene of glucosyltransferase Rgg (Dmitriev et al., 2006; Shelburne et al., 2010). CovRS mediates a general stress response to changing temperature, pH, and osmolarity (Dalton and Scott, 2004), and Ccp A and Rgg are directly linked to environmental glucose deprivation (Dmitriev et al., 2006; Shelburne et al., 2008). While CovR deletion induces a several-fold increase of ADI pathway genes, CcpA or Rgg deletions markedly induce several-log fold increases in the pathway (Dmitriev et al., 2006; Shelburne et al., 2010). These findings suggest that the ADI pathway is especially important to *S. pyogenes* under low glucose conditions. Notably, the glucose concentration in the SC of skin is much lower than that present in blood (Sylvestre et al., 2010). In this study, we investigated whether the *S. pyogenes* ADI pathway contributes to the viability and pathogenesis of an M1T1 strain under low glucose conditions and in the skin.

Results

S. pyogenes ADI pathway contributes to its viability and virulence

The *S. pyogenes* ADI pathway is comprised of ArcA, B, C, and D (Figure S1A) (Cusumano et al., 2014). ArcA, an arginine deiminase, is the first enzyme of ADI pathway, and catalyzes the irreversible hydrolysis of arginine to citrulline and ammonia. We constructed a markerless complete *arcA* deletion mutant (Δ*arcA*) using a double crossover homologous recombination technique, preserving as a control a wild-type revertant strain (Wr) from the single crossover step back to integrity of *arcA.* We first observed the time course of pH change of bacterial cultures grown under arginine-rich conditions, using phenol red as an indicator of elevated pH (Figure 1A). The wild-type (WT) *S. pyogenes* parent strain induced pH elevation in the culture medium beginning in stationary phase, whereas the *S. pyogenes* Δ*arcA* did not, confirming loss of *arcA* renders the bacterium's arginine catabolism dysfunctional. Deletion of *arcA* led to a decrease in *S. pyogenes* viability during the decline phase of stationary growth in THY broth (Figure 1B). In contrast, the WT *S. pyogenes* strain exhibited a strong increase in *arcA* gene expression and ammonium ion production occurring during stationary phase following glucose starvation (Figures 1C, 1D, and 1E). While a pH elevation was not detected during the stationary phase in THY broth, pH levels in phenol red broth supplemented with arginine were elevated above neutral pH for both the WT and Wr cultures (Figures S1B and S1C). Both WT and Wr showed the potential for long-term survival in neutral pH for at least 40 days during the decline phase, whereas the mutant strain lost viability after only 2 days (Figure S1B). These findings

indicate that *S. pyogenes* neutralizes excess protons during stationary phase by synthesizing ammonia in an ADI-dependent manner, thus promoting long term viability during the decline phase.

S. pyogenes cultured in THY broth experienced glucose starvation beginning in stationary phase. To investigate whether arginine catabolism contributed to *S. pyogenes* virulence phenotypes under such glucose starved conditions, we prepared chemically-defined medium (CDM, Table S1) without glucose, phenol red, or arginine. As a first surrogate marker of virulence, we evaluated *S. pyogenes* cytotoxicity against the cultured human keratinocyte cell line, HaCaT. We supplemented 1000 μM arginine in the CDM to match the physiological concentration present in human muscle tissue (Canepa et al., 2002). At 20 h after infection of HaCaT cells in arginine-supplemented conditions, WT and Wr showed a dose-dependent increase in cytotoxic potential compared to the Δ*arcA* mutant (Figure 1F and S1D), linking arginine catabolism to this virulence phenotype.

By metabolizing arginine, *S. pyogenes* acquires adenosine triphosphate (ATP) as an energy source, coupled to discharge of ammonium ion (Figure S1A). Intracellular acidification may affect growth and cell viability of streptococci (Dashper and Reynolds, 2000). We probed the contribution of arginine catabolism to *S. pyogenes* intracellular pH and ATP levels under low glucose conditions using CDM. No effects on the intracellular pH of *S. pyogenes* were observed 1 h, 5 h, and 15 h post-incubation in CDM (Figure S1E). Conversely, at 1 h and 5 h post-incubation, arginine catabolism contributed to the acquisition of ATP in the no glucose condition (Figure 1G), which correlated with viability of *S. pyogenes* at 5 h and 15 h post-incubation in CDM (Figure 1H). *S. pyogenes* WT in CDM at 15 h had greater viability when cultured in the presence of HaCaT cells than in their absence (Figure 1H), suggesting that ADI-dependent *S. pyogenes* cytotoxicity induces release of nutrition from damaged keratinocytes, promoting *S. pyogenes* survival.

S. pyogenes arginine catabolism changes global gene expression

We conducted RNA-seq analysis of the *S. pyogenes* strains in CDM with arginine, Arg(+), or without arginine, Arg(−), to assesses transcriptional consequences of altering the ADI pathway. Principal component analysis (PCA) showed Δ*arcA* Arg(−), Δ*arcA* Arg(+), and WT Arg(−) samples clustered together, while WT Arg(+) samples positioned clearly apart from the others (Figure 2A). Differentially expressed genes (DEGs) from comparisons of the Arg(+) and Arg(−) groups were detected only in the WT *S. pyogenes* background and not with the Δ*arcA* (Figure 2B, Datasets S1 and S2). The cumulative results indicated that arginine-dependent transcriptome changes in *S. pyogenes* occurred only in the presence of an intact ADI pathway. A heatmap using selected characteristic genes showed that upregulated genes in WT Arg(+) samples included those encoding virulence factors, such as an enzyme for maturation of the cytolysin streptolysin S (*sagB*), another cytolysin streptolysin O (*slo*), nucleases (*spd3*), and NADase (*nga*), but also genes comprising the pyrimidine biosynthesis pathway (*pyrD, pyrE*, and *pyrF*) (Figure 2C). On the other hand, cell division-associated genes (*ftsH, ftsL*, and *ftsZ*), and genes encoding F_0F_1-type ATP synthase (*atpB-H*) were downregulated in WT *S. pyogenes* in the presence of arginine.

The most well studied *S. pyogenes* two-component signal transduction system is the cluster of virulence (Cov) intracellular responder (CovR)/extracellular sensor (CovS), CovRS, which influences 15-20% of the *S. pyogenes* genome (Graham et al., 2002). CovS sensed environmental changes and transmitted to CovR via phosphorylation-dephosphorylation (Horstmann et al., 2015). Of particular interest, the *covS* gene was downregulated in WT *S. pyogenes* sensing arginine (Figure 2C, Dataset S2). To investigate whether arginine catabolism influences CovR phosphorylation, we monitored phosphorylation of the regulator using 5′Flag-CovR strain (Figure 2D). Exponential phase growth of *S. pyogenes* in THY broth showed low levels of CovR phosphorylation. For *S. pyogenes* within CDM, WT Arg(+) sample tended to show a low level of CovR phosphorylation, but no significant difference was found by the densitometric analysis (Figure 2E).

ADI pathway contributes to the development of cutaneous lesions

The SC of skin is relatively deficient in glucose (Sylvestre et al., 2010), while arginine is abundant (Kubo et al., 2013). We hypothesized that *S. pyogenes* may utilize arginine to acquire energy on the skin surface, and examined this possibility using a mouse model of epicutaneous infection (Figure 3A). By 3 days post-challenge, the skin surface of mice infected with WT or Wr *S. pyogenes* had peeled off, while it remained intact in Δ*arcA*-infected mice (Figure 3B). Furthermore, CFU recovered from skin lesions 3 days post-infection were significantly reduced in Δ*arcA*-infected mice compared to the WT or Wr (Figure 3C). Analysis of gene expression showed the WT *S. pyogenes* strain had higher *in vivo* expression of the genes encoding the streptolysin S precursor (*sagA*) and streptolysin O (*slo*), but reduced expression of the gene encoding cysteine protease SpeB (*speB*) compared to the Δ*arcA* mutant (Figure 3D). These results indicate that arginine catabolism contributes to the pathogenesis of *S. pyogenes* on the skin surface while promoting the expression of cytolysins.

To assess the ADI-dependent effects on *S. pyogenes* systemic pathogenicity, we conducted intravenous challenge of mice along with an *ex vivo* bactericidal assay using mouse blood. In both sets of experiments, there were no significant differences between WT and Δ*arcA* (Figures 3E and 3F); this arginine catabolism may not be involved in the virulence or viability of *S. pyogenes* in blood. We speculated that arginine catabolism was suppressed in blood due to high concentrations of glucose. With that in mind, we evaluated *arcA* gene expression of WT *S. pyogenes* in blood and on the skin surface by using qPCR. Using an expression level of *arcA* in the exponential phase growth in THY medium set to 1, *arcA* expression was 10 to 100 times lower in blood and 10 times greater on the skin than in the culture conditions (Figure 3G). This result suggests that the expression on the skin surface was promoted 2 to 3-log fold compared to that in blood, where low glucose concentrations are found. Expanding the repertoire of infection models, we found that in a subcutaneous mouse soft-tissue infection model which causes necrosis of fascial tissue and adjoining muscle, the Δ*arcA* showed reduced virulence compared to WT and Wr (Figure S2A), while there were no differences in virulence in another systemic challenge via intraperitoneal infection (Figure S2B). It is speculated these contrasting results reflect differences in available concentrations of glucose and arginine in localized vs. systemic disease compartments.

Next, an epicutaneous infection study was conducted using streptozotocin-induced diabetic mice. As expected, 48 h after depilation of dorsal skin, glucose levels on the skin surface in non-diabetic (wt) mice were below the detection limit (< 1 μM) in nearly all samples, while those in the diabetic mice were much higher (4 μM −70.4 μM, Figures S2C and S2D). In response to an epicutaneous infection in diabetic mice, Δ*arcA* showed comparable recovered CFU from the skin lesion to WT (Figure S2E). Both WT and Δ*arcA* in CDM showed the upregulation of *slo* gene in the presence of glucose (Figures S2F and S2G). These results suggested that the abundance of glucose on the skin surface in diabetes allows the pathogen to exhibit pathogenicity independently of arginine-catabolism, consistent with the known increased risk of *S. pyogenes* skin and soft tissue infections in patients with diabetes (Lin et al., 2011).

In our RNA-seq data *in vitro*, 4 genes associated with phosphotransferase system (PTS) were upregulated in WT under arginine-rich conditions (*ptsD, SP5448_05675, SP5448_08850, SP5448_08855*). Therefore, we evaluated the expression levels of these transporter genes 3 h post-epicutaneous infection in wt mice (Figure S3). The expression levels each gene tended to be upregulated in WT compared to the Δ*arcA* mutant. This result also suggests the skin surface of wt mice has a low glucose concentration, and *S. pyogenes* upregulates the expression of transporter genes in a manner that depends on arginine catabolism.

ADI pathway-dependent bacterial virulence was canceled in *Flg*$^{-/-}$ mice

Arginine is abundant in filaggrin, an abundant protein within the SC of skin, and filaggrin knock-out (*Flg*$^{-/-}$) mouse has markedly lower SC arginine level than corresponding wild-type (wt) mouse (Kawasaki et al., 2012; Kubo et al., 2013). The degradation of Filaggrin into amino acids occur in the SC layers by host-derived enzymes, including caspase-14, calpain 1, and bleomycin hydrolase (Hoste et al., 2011). We hypothesized that *S. pyogenes* acquires arginine from filaggrin in SC for nutritional requirements and virulence gene on the skin surface.

At baseline, it is difficult to appreciate any phenotypic differences between wt mice and *Flg*$^{-/-}$ mice (Figure 4A). However, following epicutaneous challenge assessed at 3 days post-infection, the previously observed difference of virulence between WT and Δ*arcA* disappeared in the skin of *Flg*$^{-/-}$ mice as verified at three different challenge inocula (Figure 4B). These results were corroborated with similar histopathology of the skin lesions at the 3 days post-infection time point (Figure 4C). The ArcA protein is associated with the *S. pyogenes* bacterial cell surface (Henningham et al., 2012). To confirm that *S. pyogenes* expresses ArcA during infection on the skin surface, immunofluorescence staining was performed at 24 h post-infection. Strong signals for ArcA expression were seen only in the case of *S. pyogenes* WT on the skin surface of wt mice (Figures 4D, and 4E). In *Flg*$^{-/-}$ mice, *S. pyogenes* did not appear to upregulate ArcA for arginine catabolism to achieve infection.

S. pyogenes showed different expression levels of *covS*, *arcA* and *slo* genes on the skin surface 3 h after epicutaneous infection in wt compared to *Flg*$^{-/-}$ mice (Figure S4). Since *Flg*$^{-/-}$ mouse skin exhibits enhanced permeability of stratum corneum as compared

to wt mouse skin (Kawasaki et al., 2012), these transcriptional differences might reflect differences of nutritional or stress environments.

In intestinal epithelial cells, it is thought that caspase-1 contributes to both pyroptosis and apoptosis during an inflammation (Lei-Leston et al., 2017). To investigate whether *S. pyogenes* caused programmed cell death of skin epithelial cells, immunofluorescence staining of caspase-1 was performed 24 h post-epicutaneous infection. We saw a marked decrease of caspase-1 expression in epithelial cells infected with the Δ*arcA* only in wt mice (Figures 4F and 4G). *S. pyogenes* induces keratinocyte apoptosis via SLO-mediated membrane damage (Cywes Bentley et al., 2005). In *S. pyogenes* infection of HaCaT cells with CDM, an increase in released lactate dehydrogenase (LDH) in culture supernatants indicated that SLO contributed partially to arginine catabolism-dependent cytotoxicity (Figure S5A). Next, we determined whether pyroptosis or apoptosis were induced in infected epithelial cells by measuring IL-1 β release and DNA fragmentation via TUNEL staining. Since it was difficult to discriminate between pro-IL-1β and mature IL-1β by ELISA, we assessed signaling activity using HEK-Blue IL-1β reporter cells for quantifying pyroptosis. The secretion of mature IL-1β from HaCaT cells was enhanced in both WT and Δ*slo* by arginine catabolism (Figure S5B), with SLO partially contributing to the pyroptosis phenotype, paralleling the cytolytic effect. On the other hand, in a TUNEL assay designed to detect apoptotic cells, arginine catabolism-dependent apoptosis was not observed (Figure S5C). Taken together, *S. pyogenes* SLO contributes significantly to the pyroptosis of HaCaT cells induced by arginine catabolism, while there are other *S. pyogenes* factors that are likely involved in arginine catabolism-independent pyroptosis.

Discussion

The *S. pyogenes* ADI pathway is controlled by virulence-related metabolic regulators (Dmitriev et al., 2006; Shelburne et al., 2010), and highly expressed *in vivo* (Graham et al., 2006; Hirose et al., 2019) and *ex vivo* (Graham et al., 2005; Shelburne et al., 2005). Here, we show that *S. pyogenes* ADI pathway influences virulence factor expression and contributes to keratinocyte cytotoxicity under low glucose conditions *in vitro* and subcutaneous infection *in vivo.* Our data support a model in which *S. pyogenes* utilizes arginine abundant in filaggrin of the SC can secure nutrition, survive, and produce skin infection associated with local tissue destruction.

We found that *S. pyogenes* can survive for more than 40 days if they can maintain neutral pH by metabolizing arginine during the stationary phase. This result is consistent with a previous report which proved the long-term survival potential of *S. pyogenes* in neutral pH (Savic and McShan, 2012). The abilities of *S. pyogenes* ADI pathway both energy production and protection against acid stress might greatly contribute to its viability in specialized environments such as skin.

Comparative transcriptome analysis reveals arginine catabolism-dependent gene regulation under glucose starvation. Upregulated genes in the WT strain include genes consisting pyrimidine biosynthesis pathway (*pyrD, pyrE*, and *pyrF*). In S. *pyogenes*, the ADI pathway cooperates with the pyrimidine biosynthesis pathway to acquire pyrimidine ribonucleotides

and ATP (Hirose et al., 2019). Conversely, genes encoding F_0F_1-type ATP synthase were downregulated in the WT strain compared to the Δ*arcA* mutant. Although it has been reported that the generation of ATP via the ADI pathway and a functional F_0F_1-type ATP synthase work in concert to adapt to acid stress (Cusumano and Caparon, 2015), it is speculated that *S. pyogenes* in CDM at neutral pH decreases the concomitant hydrolysis of ATP to ADP to reduce ATP consumption. Genes related to cell division (*ftsH, ftsL*, and *ftsZ*) were also downregulated in WT. *S. pyogenes*, which might prioritize the expression of cytolytic virulence factors when there are not enough local nutrition sources to proliferate.

The deletion of *covR* induces the upregulation of virulence genes contained within the streptolysin S operon (*sagABCDEFGHI*) and the *nga-slo* operon, and also shows downregulation of dipeptide permease operon (*dppABCDE*) (Shelburne et al., 2010). These findings were mirrored in our results from RNA-seq analysis. Although CovR phosphorylation enhances DNA binding of CovR (Graham et al., 2002) and CovR affects expression of 15-20% of *S. pyogenes* genes (Horstmann et al., 2015), *S. pyogenes* arginine catabolism did not significantly influence CovR phosphorylation in our assay. Taken together, these results suggest that the main mechanism of *S. pyogenes* pathogenicity in the glucose depleted condition may be dependent on acquiring ATP by catabolism of arginine.

Although transcript levels of ADI operon were reduced in serotype M1 *S. pyogenes* (MGAS5005) after human blood exposure, temporal and mild upregulation of ADI operon was observed within 90 min of blood exposure (Graham et al., 2005). These investigators also reported that the deletion of the *S. pyogenes covR* regulator led to upregulation of the ADI operon in blood. These results partly contrast with our data. However, human blood is relatively poor in arginine, while rich in glucose (Canepa et al., 2002; Sylvestre et al., 2010). Therefore, although CovRS might mediate some environmental signals in the blood and upregulate ADI operon expression, we speculate that arginine catabolism changes are not sufficient to drive pathogenesis of *S. pyogenes* in blood. In contrast, the Δ*arcA* mutant showed lower virulence compared to the WT *S. pyogenes* strain in mouse soft-tissue infection model associated with localized necrosis in adjacent muscle. This difference in pathogenicity might be explained by high concentrations (approximately 1,000 μM) of arginine in muscle tissue (Canepa et al., 2002).

In a murine model of epicutaneous infection and in our RNA-seq analysis, *S. pyogenes* WT upregulated the *arcA*, *slo*, and *sagA* genes. High expression levels of these genes were reported in *S. pyogenes* isolated directly from mouse soft tissue infection (Graham et al., 2006) and a mouse model of necrotizing fasciitis (Hirose et al., 2019). Streptolysin S is involved in cellular injury, phagocytic resistance, and virulence in murine subcutaneous infection models (Datta et al., 2005; Humar et al., 2002). The upregulation of SLO has been correlated to a high virulence *S. pyogenes* phenotype (Zhu et al., 2015). Our finding reported that ADI contributes to the expression of the *sagA* and *slo* genes might be important information for mitigating the pathogenicity of *S. pyogenes*.

The SC is the outermost layer of the epidermis and acts as the first line of structural defense against pathogens and toxins. Filaggrin, a major structural protein in the SC (Sandilands et al., 2009), contributes to the mechanical strength and integrity of the SC *in vivo* (Kawasaki

et al., 2012), and filaggrin breakdown products form natural moisturizing factors which are believed to play a major role in SC hydration (Rawlings and Harding, 2004). Arginine is a major component of filaggrin-derived natural moisturizing factors (Kubo et al., 2013). In our epicutaneous infection model with *Flg*$^{-/-}$ mice, *S. pyogenes* might more easily penetrate to reach viable epidermal cells below the SC whereupon cytotoxic factors can allow the pathogen to secure nutrition from the viable host epidermal cells. Thus, Δ*arcA* could exert pathogenesis by using ADI-independent mechanisms on the skin surface of *Flg*$^{-/-}$ mice.

The SC of skin is also rich in lipids, such as ceramides, cholesterol, and free fatty acids (Elias and Schmuth, 2009), and bacterial infection of the skin also activates the host immune response (Cogen et al., 2008) and promotes acidic pH (Proksch, 2018). In our results, there were certain differences between our *in vitro* and *in vivo* findings that could not be explained based solely on *S. pyogenes* ADI pathway activity. Further experiments will be required to confirm whether other factors are involved in the pathogenesis of *S. pyogenes* and, reveal more details about interactions between *S. pyogenes* and host skin tissue.

We revealed that *S. pyogenes* induced increased pyroptosis of HaCaT cells in a manner dependent on arginine catabolism, while almost no apoptosis was observed both dependently and independently of arginine catabolism. However, Bentley et al. reported that *S. pyogenes* SLO contributed to keratinocyte apoptosis (Cywes Bentley et al., 2005). This discrepancy may be due to the difference of the keratinocyte cell line used or nutritional conditions. Since SLO was not fully responsible for the observed pyroptosis, further exploration will be needed to fully clarify the arginine catabolism-dependent pyroptosis-inducing factors of *S. pyogenes*.

In summary, our findings suggest that *S. pyogenes* utilizes arginine from SC- derived filaggrin to adapt to glucose starvation on the skin surface. Despite the fact that arginine is a molecule that contributes to natural moisturizing of the skin, it can be simultaneously exploited by *S. pyogenes* may metabolize arginine to promote its pathogenesis.

STAR Methods text

Resource availability

Lead contact—Further information and requests for reagents may be directed to, and will be fulfilled by the corresponding author Yujiro Hirose (yujirohirose@dent.osaka-u.ac.jp).

Materials availability—This study did not generate new unique reagents.

Data and code availability—Raw reads determined in this work were deposited into the DDBJ sequence read archive (DRA) under accession number DRA009112.

Experimental model and subject details

Bacterial strains and culture conditions—*Streptococcus pyogenes* M1T1 strain 5448 (accession: CP008776.1) was isolated from a patient with toxic shock syndrome and necrotizing fasciitis that is genetically representative of a globally disseminated clone associated with invasive *S. pyogenes* infections (Kansal et al., 2000). *S. pyogenes* strains

were grown at 37°C in a screw-cap glass tube (Pyrex; Iwaki Glass, Tokyo, Japan) filled with Todd-Hewitt broth (BD Biosciences, San Jose, CA, USA) supplemented with 0.2% yeast extract (BD Bioscience) (THY broth) in an ambient atmosphere and standing cultures. To obtain cultures for experiments and observe pH change, overnight cultures of *S.pyogenes* were back diluted 1:50 into fresh THY broth or phenol red broth (Sigma Aldrich, St Louis, MO, USA) supplemented with 30 mM arginine. CFUs were determined by plating diluted samples on THY blood agar.

Escherichia coli strain XL-10 Gold (Agilent Technologies, Santa Clara, CA, USA) was used as a host for derivatives of plasmids pSET4s (Takamatsu et al., 2001) and pQE30 (Qiagen, Hilden, Germany). *E. coli* strains were cultured in Luria-Bertani medium (Nacalai Tesque, Kyoto, Japan) at 37°C with agitation. For selection and maintenance of strains, antibiotics were added to the medium at the following concentrations: spectinomycin, 100 μg/mL for *S. pyogenes* and *E. coli*: carbenicillin, 100 μg/mL for *E. coli.*

Construction of mutant strains—An in-frame *arcA* deletion mutant (Δ*arcA*) and its revertant strain (Wr) with a background of strain 5448 (WT) were constructed using the pSET4s temperature-sensitive shuttle vector, as previously reported (Nakata et al., 2011). A pSET4-ArcAKO plasmid harboring the DNA fragment, in which upstream and downstream regions of *arcA* were linked by overlapping PCR, was electroporated into strain 5448 and grown in the presence of spectinomycin. The plasmid was then integrated into the chromosome via first allelic replacement at 37°C, after which it was cultured at 28°C without antibiotics to induce the second allelic replacement. The deletion of *arcA* was confirmed by site-specific PCR using purified genomic DNA. Primers are listed in Table S2.

Cell culture and media—We used the immortal human keratinocyte line, HaCaT cells. HaCaT cells were cultured in Dulbecco's Modified Eagle Media (DMEM, Cat#: 10-013-CV, Corning, NY, USA), with 10% Fetal Bovine Serum (Cat# 97068-085, VWR International LLC, Radnor, USA). The cell culture was maintained in a humidified 5% CO_2 atmosphere at 37°C. The cells were cultured to around 70% confluence. To subculture cells, adherent cells were rinsed with PBS without calcium and magnesium, and detached by using trypsin/EDTA solution (0.05% trypsin, 0.53m EDTA) for ~10 min, added fresh culture medium, centrifuged, resuspended cells in fresh culture medium, and dispensed into new culture vessels. For all experiments, freshly trypsinized cells were seeded at a density of ~1×10^5 cells/cm^2 one day prior to bacterial infection

Murine model of epicutaneous and intravenous infections—All mouse experiments were conducted in accordance with animal protocols approved by the Animal Care and Use Committee of Osaka University Graduate School of Dentistry (30-011-0) and University of California San Diego Institutional Animal Care and Use Committee (IACUC). The lack of filaggrin-null mouse strain (B6.Cg-Flg<tm1>, RBRC05850) was provided by RIKEN BRC through the National Bio-Resource Project of the MEXT, Japan.

Epicutaneous infections were performed using a previously reported with minor modifications (Nakamura et al., 2013; Sumitomo et al., 2018). Briefly, bacterial cultures during exponential phase were centrifuged, washed with and resuspended in PBS. Dorsal

skin of C57BL/6 wild-type (wt) mice (6- to 7-week-old, both female and male; Japan SLC, Shizuoka, Japan) and the lack of filaggrin-null (*Flg*$^{-/-}$) mice (Kawasaki et al., 2012) (6- to 7-week-old, both female and male) was depilated 2 days before infection. A bacterial suspension (5×10^5-10^7 CFU in 100 μL PBS) was placed on a 1 × 1 cm patch of sterile gauze, which is secured to the shaved skin with a transparent bio-occlusive dressing. At 3 hours post-infection, bacteria on the skin surface were collected by using a stainless dental scaler, then bacterial RNA was extracted and quantified by qPCR as described above. At 3 days post-infection, cutaneous tissue was excised for histopathologic analyses and assessment of bacterial burden. Cutaneous tissue samples were obtained and fixed with formalin, then embedded in paraffin, sectioned, and subjected to hematoxylin and eosin (HE) staining. Bacterial counts in cutaneous tissue homogenates were determined after plating serial dilutions, with those in the cutaneous tissue corrected for differences in tissue weight.

For intravenous infection, C57BL/6 wild-type mice (6- to 7-week-old, both female and male; Japan SLC) were intravenously infected with 2×10^6 CFU of *S. pyogenes* during exponential phase, and survival was monitored for 14 days.

Mouse model of *S. pyogenes* necrotizing skin infection—Invasiveness of *S. pyogenes* in mouse skin was measured by modification of a previously described *S. pyogenes* infection model (Nizet et al., 2001). All mouse experiments were conducted in accordance with animal protocols approved by the Animal Care and Use Committee of Osaka University Graduate School of Dentistry (30-011-0). The CD-1 (S1c: ICR) mice (6 weeks old, female; Japan SLC, Shizuoka, Japan) were shaved and hair removed by chemical depilation (Veet, Oxy Reckit Benckiser, Chartes, France). *S. pyogenes* were cultured until the log phase (OD_{600} = 0.5~0.6), and adjusted 1×10^7 CFU in 200 μL of PBS were injected subcutaneously. Areas with ulcer were defined as lesions and areas were measured daily for up to 3 days after infection.

Mouse model of intraperitoneal infection—Intraperitoneal infections were performed using a previously reported with minor modifications (Valdes et al., 2016). C57BL/6 wild-type (wt) mice (6- to 7-week-old, both female and male; Japan SLC, Shizuoka, Japan) and the lack of filaggrin-null (*Flg*$^{-/-}$) mice (Kawasaki et al., 2012) (6- to 7-week-old, both female and male) were intraperitoneally injected with 2.5×10^8 CFU in 100 μL of PBS. Mouse survival was monitored for 14 days.

Streptozotocin-induced diabetic mice—To induce diabetes mellitus, C57BL/6 male mice (4-week-old) were injected i.p. with streptozotocin (Adipogen, San Diego, CA, USA) at 80 mg/kg/dose in 200 μL of 0.1 M citrate buffer daily for 4 days (Patras et al., 2020). Control mice received 4 daily treatments of 200 μL of 0.1 M citrate buffer. Mice were weighed weekly thereafter. The concentration of blood glucose 7-week-old mice was determined 24 h prior to infection. Sample glucose was determined using an AimStrip Plus blood glucose meter kit (Germaine Labs, Indianapolis, IN, USA).

Method details

Quantitative real-time PCR (qPCR)—Bacterial cultures during exponential phase (OD_{600} = 0.5-0.6), early stationary phase (OD_{600} = 1.2), or decline phase (overnight culture) were centrifuged and immediately placed into RNAprotect Bacteria Reagent (Qiagen) prior to RNA isolation. In the RNA isolation from *S. pyogenes* cultured within CDM, bacterial cultures during exponential phase (OD_{600} = 0.5-0.6) were centrifuged, resuspended into CDM, incubated in a screw cap glass tube (Pyrex; Iwaki Glass, Tokyo, Japan) for 1 h at 37°C, and and immediately placed into RNAprotect Bacteria Reagent. *S. pyogenes* was resuspended into lysing Matrix B microtubes containing 0.1-mm silica spheres (Qbiogene, Carlsbad, CA, USA) with RLT lysis buffer (RNeasy Mini Kit; Qiagen), and homogenized at 6,500 rpm for 60 s using the MagNA Lyser (Roche Molecular Diagnostic, Mannheim, Germany). RNA was isolated from the lysate with RNeasy Mini Kit according to the manufacturer's guidelines, and then cDNA was synthesized using a Superscript VILO cDNA synthesis kit (Thermo Fisher Scientific, Waltham, MA, USA). Real-time reverse transcription PCR analysis was performed using a StepOnePlus real-time PCR system (Applied Biosystems, Foster City, CA, USA) and Toyobo SYBR green RT-PCR master mix kit (Toyobo Life Science, Osaka, Japan). Data for *16S rRNA* or *rpoB* were used as the internal control. Primers used for qPCR are listed in Table S2.

Measurement of glucose and ammonium ion concentrations—Culture supernatant at each growth phase obtained from *S. pyogenes* WT and Δ*arcA* cultured in THY broth was filtered through a 0.22 μm membrane, then and directly analyzed with BioProfile® FLEX2 analyzer following manufacturer's instruction (Nova Biomedical, Inc., Waltham, MA, USA).

Measurement of extracellular pH—For phenol red broth (Sigma Aldrich, St Louis, MO, USA) supplemented with 30 mM arginine, culture supernatant at each point was measured the absorbance at 550 nm. A calibration curve was determined in phenol red broth which adjusted to pH values ranging from 4 to 10. The pH values were assessed up to 40 days in the sample which included surviving bacteria. For THY broth, culture supernatant at each point was supplemented with 5 mg/mL phenol red and the absorbance was measured at 550 nm. A calibration curve was determined in THY broth which was supplemented with 5 mg/mL phenol red and adjusted to pH values ranging from 4 to 10.

Measurement of intracellular pH—The cytosolic pH of *S. pyogenes* was determined based on the previously described fluorescent probe method (Do et al., 2019). Briefly, *S. pyogenes* grown to log phase of growth in THY broth were centrifugated, washed in 150 mM NaCl, and resuspended in 50 mM HEPES buffer (pH 8.0). The cells were then incubated for 20 min at 37 °C in the presence of 10 μM carboxyfluorescein diacetate succinimidyl ester (cFDASE, Invitrogen, Grand Island, NY, USA). cFDASE is hydrolyzed to carboxyfluorescein succinimidyl ester (cFSE) in the cell and subsequently conjugated to aliphatic amines of the intracellular proteins. After incubation, cells were washed and suspended in 50 mM potassium phosphate buffer (pH 7.5). To eliminate nonconjugated cFSE, cells were incubated with 10 mM glucose for 30 min at 30 °C. Subsequently, *S. pyogenes* were washed, and suspended, and incubated in CDM at 37°C within a screw-cap

glass tube. At 1 h, 5 h, and 15 h post-incubation, fluorescence intensities were determined with an excitation spectrum of 400-500 nm wavelength range that includes excitation wavelengths 490 nm (pH-sensitive) and 435 nm (pH-insensitive) (Spark 10M; TEKAN, Männedorf, Switzerland). Emission was determined at 520 nm. The ratio of the emission resulting from excitation at 490 and 435 nm obtained for both cell suspension (C) and filtrate (F) was calculated as R 490/435 = (C490 - F490)/(C 435 - F435). A calibration curve was determined in CDM adjusted to pH values ranging from 5.5 to 8.0 and a cubic equation for the ratio value was determined. Intracellular pH values of *S. pyogenes* were calculated using the cubic equation from the calibration curve.

Infection of HaCaT cells with *S. pyogenes*—The composition of Chemically Defined Medium (CDM) is shown in Table S1. *S. pyogenes* in log phase growth in THY broth were centrifuged and resuspended into CDM supplemented with or without 1000 μM arginine. HaCaT cells were infected with *S. pyogenes* (MOI = 500). At 20 h post-incubation, supernatants were collected by centrifugation and analyzed for cytotoxicity assays, IL-1β signaling assay, and cells were used for the apoptosis determination.

Cytotoxicity assays—Cell viability was assessed using the LIVE/DEAD® Viability/ Cytotoxicity Kit (Thermo Fisher Scientific). LDH activity in the culture supernatant was measured by using LDH Assay Kit-WST (Dojindo, Kumamoto, Japan). At 1 h, 5 h, and 15 h post-infection, the bacterial count in CDM with cultured HaCaT cells was evaluated by combining CFUs from supernatant and those from associated with HaCaT cells. To determine bacterial association, HaCaT cells were harvested with PBS containing 0.05% trypsin and 0.025% Triton X-100.

Measurement of intracellular ATP levels—At 1 h, 5 h, and 15 h post-incubation in CDM, the intracellular ATP levels of *S. pyogenes* were also evaluated by an ATP-bioluminescent assay using Kinshiro (TOYO B-Net, Tokyo, Japan) according to manufacturer's instructions. Briefly, ATP extractant solution was added to equal amount of the mixture of CDM and *S. pyogenes.* After the incubation for 10 s at room temperature, 100μL samples were mixed with equal amount of bioluminescent reagent, and bioluminescence was measured with a luminometer (Infinite 200 Pro multiplate reader, TEKAN, Männedorf, Switzerland), immediately. After establishing of the calibration curve, the ATP concentrations in the samples were determined, and the percentage of ATP levels for *S. pyogenes* at 0 h post-incubation was calculated.

RNA-seq and data analysis—Bacterial cultures during exponential phase were centrifuged, resuspended into CDM, and incubated in a screw-cap glass tube (Pyrex; Iwaki Glass, Tokyo, Japan) for 1 h at 37°C. RNA samples of *S. pyogenes* were obtained after incubation, as described above. RNA integrity was assessed using a 2100 Bioanalyzer (Agilent Technologies, Santa Clara, CA, USA). For RNA-seq, bacterial RNA was treated for rRNA removal using a Ribo-Zero rRNA removal kit (Illumina Inc., San Diego, CA, USA). RNA-seq libraries were created using a TruSeq RNA Sample Prep kit, v2 (Illumina Inc.), according to the manufacturer's recommendations. Libraries were sequenced using Illumina HiSeq 2500 systems, with 75-bp single-end reads. RNA-seq reads were mapped against

the *S. pyogenes* strain 5448 genome using the commercially available CLC Genomics workbench, v. 9.5.2 (CLC Bio, Aarhus, Denmark). Global analyses of RNA-seq expression data were performed using iDEP (Ge et al., 2018), with the FPKM value of each sample. We classified the differentially expressed genes (DEGs) into functional categories based on the bacterial bioinformatics database and analysis resource PATRIC (Wattam et al., 2017). The heatmap was visualized by use of the web tool ClustVis (Metsalu and Vilo, 2015) with default parameters.

Phos-tag western blotting for the detection of phosphorylated CovR—For this experiment, we constructed in-frame 5'-3xflag-tagged *covR* insertion mutants (5'Flag-CovR) of WT and Δ*arcA*. Utilizing strain 5448 genome DNA as a template, two other DNA fragments were amplified using primer sets 5'Flag-CovRF1 and 5'Flag-CovRR1, or 5'Flag-CovRF1 and 5'Flag-CovRR1 (Table S2). Then, two fragments were PCR-linked, and a fragment encoding 5'-3xflag-tagged *covR* was created. Finally, a pSET4-5'Flag-CovR plasmid harboring 5'-3xflag-tagged *covR* was transformed to generate 5'Flag-CovR strain, as described above.

Bacterial cultures during exponential phase were centrifuged, resuspended into CDM, and incubated in a screw-cap glass tube for 1 h at 37°C. To extract total protein from *S. pyogenes*, we prepared our original lysis buffer which contains 10 U mutanolysin (Sigma Aldrich), cOmplete, EDTA (+) Protease Inhibitor Cocktail (Roche Molecular Diagnostic, Pleasanton, CA, USA), and PhosSTOP™ (Roche Molecular Diagnostic) in PBS. Bacterial cultures in THY broth during exponential phase or the mixture of CDM and *S. pyogenes* were centrifuged, and resuspended into lysing Matrix B microtubes containing 0.1-mm silica spheres with our original lysis buffer, and homogenized at 6,500 rpm for 30 s using the MagNA Lyser (Roche Molecular Diagnostic). The lysates were centrifuged, and the supernatants were applied to SDS-PAGE (Phos-tag SuperSep™ Phos-tag™ Gels; Wako Pure Chemical Industries, Osaka, Japan). The gel was transferred onto the Immobilon-FL PVDF (Millipore, Billerica, MA, USA) and phosphorylated CovR was detected by Anti-DDDDK-tag mAb-Alexa Fluor® 488 (MBL, Nagoya, Japan). Labeled proteins were visualized using Amersham Typhoon RGB Biomolecular Imager (Amersham Biosciences-GE Healthcare, Piscataway, NJ, USA). Relative percentage of phosphorylated CovR were calculated using ImageQuant software (Molecular Dynamics, Sunnyvale, CA, USA).

Detection of glucose concentration on the skin—At 48 h after depilation of dorsal skin of mice, a cup was placed on the skin and 100 μL PBS was injected. Then the skin was scratched by disposable inoculating loops and the sample was collected. Glucose concentration was measured with Glucose Colorimetric Assay Kit II (Biovision, Milpitas, CA, USA) following manufacturer's instruction.

Blood bactericidal assay—Heparinized mouse blood (190 μL) and exponential phase bacteria (1.5×10^6 CFU in 10 μL of PBS) were mixed in 96-well plates and incubated at 37°C in 5% CO_2 for 1, 2, or 3 hours. Viable cell counts were determined by plating diluted samples on THY blood agar. At 3 hours post mixing, bacterial RNA in blood were also isolated for qPCR. Blood samples were mixed with the component of RNAprotect® Animal Blood Tubes (Qiagen), and centrifuged. Pellets were placed in lysing Matrix D microtubes

containing 1.4-mm silica spheres (Qbiogene) with RLT lysis buffer (RNeasy kit; Qiagen) and homogenized at 6,500 rpm for 45 s using a MagNA lyser. The lysate was centrifuged, and the obtained pellet was resuspended in lysing Matrix B microtubes containing 0.1-mm silica spheres (Qbiogene) with the RLT lysis buffer and homogenized at 6,500 rpm for 60 s using the MagNA lyser. The final lysate was centrifuged and bacterial RNA was isolated from the collected supernatant with a RNeasy kit, according to the manufacturer's guidelines.

Immunofluorescence staining—Paraffin sections of cutaneous tissues of non-infected mice were subjected to immunofluorescence staining to detect filaggrin of mice. Following deparaffinization, sections in a 10 mM sodium citrate solution (pH 6.0) were heated for 5 min in a pressure cooker to retrieve the antigens.

Paraffin sections of cutaneous tissues at 24 hours post-infection were subjected to immunofluorescence staining to detect *S. pyogenes*, bacterial ArcA, and caspase-1 of host cells. ArcA was detected with rabbit antiserum against recombinant ArcA proteins which purified from pQE30-ArcA transformed XL10-Gold by using Ni-NTA resin. Following deparaffinization, sections in a 10 mM sodium citrate solution (pH 6.0) were heated for 5 min in a pressure cooker. To visualize *S. pyogenes* and bacterial ArcA, goat polyclonal to *S. pyogenes* carbohydrate (1/100; Abcam, Cambridge, MA, USA) and rabbit antiserum against recombinant ArcA (1/100) were applied after blocking with PBS containing 2% normal donkey serum. To visualize *S. pyogenes* and caspase-1 of host cells, goat polyclonal to *S. pyogenes* carbohydrate (1/100) and rabbit polyclonal to caspase-1 (1/100; GeneTex, Irvine, CA, USA) were applied after blocking with PBS containing 2% normal donkey serum. Then, to visualize both of them, donkey anti-Goat IgG Alexa Fluor 594 (1/200; Thermo Fisher Scientific), and donkey anti-Rabbit IgG H&L Alexa Fluor 488 (1/200; Abcam) were applied as the secondary antibody.

Finally, all sections were mounted with ProLong Gold (Thermo Fisher Scientific). Stained tissue sections were examined with a Keyence microscope (Keyence Japan, Tokyo, Japan).

IL-1β signaling assay—Stably transfected HEK-Blue IL-1β reporter cells (InvivoGen, San Diego, CA, USA) (40,000 cells per well in 96-well plates), were stimulated at 37°C in 5% CO_2 with 50 μL of supernatants from infected HaCaT cells. After 18 h stimulation, supernatants from the HEK-Blue cells were analyzed for secreted alkaline phosphatase activity by the addition of 50 μL of supernatants onto 150 μL of Quanti-Blue reagent (Invivogen) and monitoring the optical density at 620 nm via EnSpire plate reader (PerkinElmer).

Apoptosis determination by Terminal transferase deoxytidyl uridine end labeling (TUNEL) staining—At 20 h post-incubation, detection of apoptosis by TUNEL was performed using Click-iT Plus TUNEL Assay Kit (Alexa Fluor 488) (Thermo Fisher Scientific, Waltham, MA, USA) following manufacturer's instruction. HaCaT cells were cultured and infected on precoated poly-L-lysine-chamber slide (Nunc Lab-Tek II Chamber Slide System) (Thermo Fisher Scientific). As a control, apoptosis of HaCaT cells were induced by treating with 0.5 μM staurosporine for 4 hours to induce apoptosis. Cover

slips were mounted on slide glasses with ProLong Gold Antifade Reagent with DAPI (Thermo Fisher Scientific). The number of TUNEL-positive and DAPI-stained nuclei were determined and the apoptosis percentage was expressed as the ratio between TUNEL-positive and DAPI-stained nuclei. Six fields per condition (100 cells each) were observed. Cells were visualized using a Zeiss Axio Observer.D1 fluorescence microscope.

Quantification and statistical analysis

Statistical analysis was performed using GraphPad Prism version 7.0 (GraphPad Software Inc., La Jolla, CA, USA). Kruskal-Wallis test with Dunn's post hoc test was used for multiple comparisons. Differences between groups were analyzed using a Mann-Whitney U test. A Mouse survival was analyzed with a log-rank test. Sample sizes and p values are indicated in figure legends.

Supplementary Material

Refer to Web version on PubMed Central for supplementary material.

Acknowledgments

We express our appreciation to Dr. T. Sekizaki and Dr. D. Takamatsu for providing the pSET4s plasmid, Dr. Riestra for providing IL-1β reporter cells, and Dr. Choi for providing HaCaT cells. We also thank Dr. Y. Nakamura, Dr. J. Hisatsune, and Dr. N. Takemoto for the advice on the experimental procedure and technique.

We acknowledge the NGS core facility of the Genome Information Research Center at the Research Institute for Microbial Diseases of Osaka University for their support with RNA sequencing and data analysis.

This study was supported in part by AMED (JP19fk0108044, JP19fm0208007, 20fk0108130h0301), Japanese Society for the Promotion of Science (JSPS) KAKENHI (grant numbers 16K15787, 19H03825, 19K22710, and 20K18474), JSPS Overseas Research Fellowships, Takeda Science Foundation, Japanese Association for Oral Biology Grant in Aid for Young Scientists, SECOM Science and Technology Foundation, The Naito Foundation, and Kobayashi International Scholarship Foundation. The funders had no role in study design, data collection or analysis, decision to publish, or preparation of the manuscript.

References

Abdelal AT (1979). Arginine catabolism by microorganisms. Annu Rev Microbiol. 33, 139–168. [PubMed: 386920]

Canepa A, Filho JC, Gutierrez A, Carrea A, Forsberg AM, Nilsson E, Verrina E, Perfumo F, and Bergstrom J (2002). Free amino acids in plasma, red blood cells, polymorphonuclear leukocytes, and muscle in normal and uraemic children. Nephrol Dial Transplant. 17, 413–421. [PubMed: 11865086]

Chatellier S, Ihendyane N, Kansal RG, Khambaty F, Basma H, Norrby-Teglund A, Low DE, McGeer A, and Kotb M (2000). Genetic relatedness and superantigen expression in group A *streptococcus* serotype M1 isolates from patients with severe and nonsevere invasive diseases. Infect Immun. 68, 3523–3534. [PubMed: 10816507]

Cogen AL, Nizet V, and Gallo RL (2008). Skin microbiota: a source of disease or defence? Br J Dermatol. 158, 442–455. [PubMed: 18275522]

Cotter PD, and Hill C (2003). Surviving the acid test: responses of gram-positive bacteria to low pH. Microbiol Mol Biol Rev. 67, 429–453. [PubMed: 12966143]

Cunningham MW (2000). Pathogenesis of group A streptococcal infections. Clin Microbiol Rev. 13, 470–511. [PubMed: 10885988]

Cusumano ZT, and Caparon MG (2015). Citrulline protects *Streptococcus pyogenes* from acid stress using the arginine deiminase pathway and the F1Fo-ATPase. J Bacteriol. 197, 1288–1296. [PubMed: 25645553]

Cusumano ZT, Watson ME Jr., and Caparon MG (2014). *Streptococcus pyogenes* arginine and citrulline catabolism promotes infection and modulates innate immunity. Infect Immun. 82, 233–242. [PubMed: 24144727]

Cywes Bentley C, Hakansson A, Christianson J, and Wessels MR (2005). Extracellular group A Streptococcus induces keratinocyte apoptosis by dysregulating calcium signalling. Cell Microbiol. 7, 945–955. [PubMed: 15953027]

Dalton TL, and Scott JR (2004). CovS inactivates CovR and is required for growth under conditions of general stress in *Streptococcus pyogenes*. J Bacteriol. 186, 3928–3937. [PubMed: 15175307]

Dashper SG, and Reynolds EC (2000). Effects of organic acid anions on growth, glycolysis, and intracellular pH of oral streptococci. J Dent Res. 79, 90–96. [PubMed: 10690666]

Datta V, Myskowski SM, Kwinn LA, Chiem DN, Varki N, Kansal RG, Kotb M, and Nizet V (2005). Mutational analysis of the group A streptococcal operon encoding streptolysin S and its virulence role in invasive infection. Mol Microbiol. 56, 681–695. [PubMed: 15819624]

Dmitriev AV, McDowell EJ, Kappeler KV, Chaussee MA, Rieck LD, and Chaussee MS (2006). The Rgg regulator of *Streptococcus pyogenes* influences utilization of nonglucose carbohydrates, prophage induction, and expression of the NAD-glycohydrolase virulence operon. J Bacteriol. 188, 7230–7241. [PubMed: 17015662]

Do H, Makthal N, VanderWal AR, Saavedra MO, Olsen RJ, Musser JM, and Kumaraswami M (2019). Environmental pH and peptide signaling control virulence of *Streptococcus pyogenes* via a quorumsensing pathway. Nat Commun. 10, 2586. [PubMed: 31197146]

Elias PM, and Schmuth M (2009). Abnormal skin barrier in the etiopathogenesis of atopic dermatitis. Curr Allergy Asthma Rep. 9, 265–272. [PubMed: 19656472]

Falugi F, Zingaretti C, Pinto V, Mariani M, Amodeo L, Manetti AG, Capo S, Musser JM, Orefici G, Margarit I, et al. (2008). Sequence variation in group A *Streptococcus* pili and association of pilus backbone types with lancefield T serotypes. J Infect Dis. 198, 1834–1841. [PubMed: 18928376]

Ge SX, Son EW, and Yao R (2018). iDEP: an integrated web application for differential expression and pathway analysis of RNA-Seq data. BMC Bioinformatics. 19, 534. [PubMed: 30567491]

Graham MR, Smoot LM, Migliaccio CA, Virtaneva K, Sturdevant DE, Porcella SF, Federle MJ, Adams GJ, Scott JR, and Musser JM (2002). Virulence control in group A *Streptococcus* by a two-component gene regulatory system: global expression profiling and *in vivo* infection modeling. Proc Natl Acad Sci U S A. 99, 13855–13860. [PubMed: 12370433]

Graham MR, Virtaneva K, Porcella SF, Barry WT, Gowen BB, Johnson CR, Wright FA, and Musser JM (2005). Group A *Streptococcus* transcriptome dynamics during growth in human blood reveals bacterial adaptive and survival strategies. Am J Pathol. 166, 455–465. [PubMed: 15681829]

Graham MR, Virtaneva K, Porcella SF, Gardner DJ, Long RD, Welty DM, Barry WT, Johnson CA, Parkins LD, Wright FA, et al. (2006). Analysis of the transcriptome of group A *Streptococcus* in mouse soft tissue infection. Am J Pathol. 169, 927–942. [PubMed: 16936267]

Henningham A, Chiarot E, Gillen CM, Cole JN, Rohde M, Fulde M, Ramachandran V, Cork AJ, Hartas J, Magor G, et al. (2012). Conserved anchorless surface proteins as group A streptococcal vaccine candidates. J Mol Med (Berl). 90, 1197–1207. [PubMed: 22527883]

Hirose Y, Yamaguchi M, Okuzaki D, Motooka D, Hamamoto FL, Hanada T, Sumitomo T, Nakata M, and Kawabata S (2019). *Streptococcus pyogenes* Transcriptome Changes in the Inflammatory Environment of Necrotizing Fasciitis. Appl Environ Microbiol. 85, e01428–01419. [PubMed: 31471300]

Horstmann N, Sahasrabhojane P, Saldana M, Ajami NJ, Flores AR, Sumby P, Liu CG, Yao H, Su X, Thompson E, et al. (2015). Characterization of the effect of the histidine kinase CovS on response regulator phosphorylation in group A *Streptococcus*. Infect Immun. 83, 1068–1077. [PubMed: 25561708]

Hoste E, Kemperman P, Devos M, Denecker G, Kezic S, Yau N, Gilbert B, Lippens S, De Groote P, Roelandt R, et al. (2011). Caspase-14 is required for filaggrin degradation to natural moisturizing factors in the skin. J Invest Dermatol. 131, 2233–2241. [PubMed: 21654840]

Humar D, Datta V, Bast DJ, Beall B, De Azavedo JC, and Nizet V (2002). Streptolysin S and necrotising infections produced by group G *Streptococcus*. Lancet. 359, 124–129. [PubMed: 11809255]

Kansal RG, McGeer A, Low DE, Norrby-Teglund A, and Kotb M (2000). Inverse relation between disease severity and expression of the streptococcal cysteine protease, SpeB, among clonal M1T1 isolates recovered from invasive group A streptococcal infection cases. Infect Immun. 68, 6362–6369. [PubMed: 11035746]

Kawasaki H, Nagao K, Kubo A, Hata T, Shimizu A, Mizuno H, Yamada T, and Amagai M (2012). Altered stratum comeum barrier and enhanced percutaneous immune responses in filaggrin-null mice. J Allergy Clin Immunol. 129, 1538–1546. [PubMed: 22409988]

Kubo A, Ishizaki I, Kubo A, Kawasaki H, Nagao K, Ohashi Y, and Amagai M (2013). The stratum corneum comprises three layers with distinct metal-ion barrier properties. Sci Rep. 3, 1731. [PubMed: 23615774]

Lei-Leston AC, Murphy AG, and Maloy KJ (2017). Epithelial Cell Inflammasomes in Intestinal Immunity and Inflammation. Front Immunol. 8, 1168. [PubMed: 28979266]

Lin JN, Chang LL, Lai CH, Lin HH, and Chen YH (2011). Clinical and molecular characteristics of invasive and noninvasive skin and soft tissue infections caused by group A *Streptococcus*. J Clin Microbiol. 49, 3632–3637. [PubMed: 21865425]

Lynskey NN, Jauneikaite E, Li HK, Zhi X, Turner CE, Mosavie M, Pearson M, Asai M, Lobkowicz L, Chow JY, et al. (2019). Emergence of dominant toxigenic M1T1 *Streptococcus pyogenes* clone during increased scarlet fever activity in England: a population-based molecular epidemiological study. Lancet Infect Dis. 19, 1209–1218. [PubMed: 31519541]

Metsalu T, and Vilo J (2015). ClustVis: a web tool for visualizing clustering of multivariate data using Principal Component Analysis and heatmap. Nucleic Acids Res. 43, W566–570. [PubMed: 25969447]

Nakamura Y, Oscherwitz J, Cease KB, Chan SM, Munoz-Planillo R, Hasegawa M, Villaruz AE, Cheung GY, McGavin MJ, Travers JB, et al. (2013). *Staphylococcus* δ-toxin induces allergic skin disease by activating mast cells. Nature. 503, 397–401. [PubMed: 24172897]

Nakata M, Kimura KR, Sumitomo T, Wada S, Sugauchi A, Oiki E, Higashino M, Kreikemeyer B, Podbielski A, Okahashi N, et al. (2011). Assembly mechanism of FCT region type 1 pili in serotype M6 *Streptococcus pyogenes*. J Biol Chem. 286, 37566–37577. [PubMed: 21880740]

Nizet V, Ohtake T, Lauth X, Trowbridge J, Rudisill J, Dorschner RA, Pestonjamasp V, Piraino J, Huttner K, and Gallo RL (2001). Innate antimicrobial peptide protects the skin from invasive bacterial infection. Nature. 414, 454–457. [PubMed: 11719807]

Patras KA, Coady A, Babu P, Shing SR, Ha AD, Rooholfada E, Brandt SL, Geriak M, Gallo RL, and Nizet V (2020). Host Cathelicidin Exacerbates Group B *Streptococcus* Urinary Tract Infection, mSphere. 5, e00932–00919.

Proksch E (2018). pH in nature, humans and skin. J Dermatol. 45, 1044–1052. [PubMed: 29863755]

Rawlings AV, and Harding CR (2004). Moisturization and skin barrier function. Dermatol Ther. 17 Suppl 1, 43–48. [PubMed: 14728698]

Sandilands A, Sutherland C, Irvine AD, and McLean WH (2009). Filaggrin in the frontline: role in skin barrier function and disease. J Cell Sci. 122, 1285–1294. [PubMed: 19386895]

Savic DJ, and McShan WM (2012). Long-term survival of *Streptococcus pyogenes* in rich media is pH-dependent. Microbiology. 158, 1428–1436. [PubMed: 22361943]

Shelburne SA 3rd, Sumby P, Sitkiewicz I, Granville C, DeLeo FR, and Musser JM (2005). Central role of a bacterial two-component gene regulatory system of previously unknown function in pathogen persistence in human saliva. Proc Natl Acad Sci U S A. 102, 16037–16042. [PubMed: 16249338]

Shelburne SA, Keith D, Horstmann N, Sumby P, Davenport MT, Graviss EA, Brennan RG, and Musser JM (2008). A direct link between carbohydrate utilization and virulence in the major human pathogen group A *Streptococcus*. Proc Natl Acad Sci U S A. 105, 1698–1703. [PubMed: 18230719]

Shelburne SA, Olsen RJ, Suber B, Sahasrabhojane P, Sumby P, Brennan RG, and Musser JM (2010). A combination of independent transcriptional regulators shapes bacterial virulence gene expression during infection. PLoS Pathog. 6, e1000817. [PubMed: 20333240]

Sumitomo T, Mori Y, Nakamura Y, Honda-Ogawa M, Nakagawa S, Yamaguchi M, Matsue H, Terao Y, Nakata M, and Kawabata S (2018). Streptococcal Cysteine Protease-Mediated Cleavage of Desmogleins Is Involved in the Pathogenesis of Cutaneous Infection. Front Cell Infect Microbiol. 8, 10. [PubMed: 29416987]

Sylvestre JP, Bouissou CC, Guy RH, and Delgado-Charro MB (2010). Extraction and quantification of amino acids in human stratum corneum *in vivo*. Br J Dermatol. 163, 458–465. [PubMed: 20394632]

Takamatsu D, Osaki M, and Sekizaki T (2001). Thermosensitive suicide vectors for gene replacement in *Streptococcus suis*. Plasmid. 46, 140–148. [PubMed: 11591139]

Valdes KM, Sundar GS, Vega LA, Belew AT, Islam E, Binet R, El-Sayed NM, Le Breton Y, and McIver KS (2016). The *fruRBA* Operon Is Necessary for Group A Streptococcal Growth in Fructose and for Resistance to Neutrophil Killing during Growth in Whole Human Blood. Infect Immun. 84, 1016–1031. [PubMed: 26787724]

Walker MJ, Barnett TC, McArthur JD, Cole JN, Gillen CM, Henningham A, Sriprakash KS, Sanderson-Smith ML, and Nizet V (2014). Disease manifestations and pathogenic mechanisms of Group A *Streptococcus*. Clin Microbiol Rev. 27, 264–301. [PubMed: 24696436]

Wattam AR, Davis JJ, Assaf R, Boisvert S, Brettin T, Bun C, Conrad N, Dietrich EM, Disz T, Gabbard JL, et al. (2017). Improvements to PATRIC, the all-bacterial Bioinformatics Database and Analysis Resource Center. Nucleic Acids Res. 45, D535–D542. [PubMed: 27899627]

Zhu L, Olsen RJ, Nasser W, Beres SB, Vuopio J, Kristinsson KG, Gottfredsson M, Porter AR, DeLeo FR, and Musser JM (2015). A molecular trigger for intercontinental epidemics of group A *Streptococcus*. J Clin Invest. 125, 3545–3559. [PubMed: 26258415]

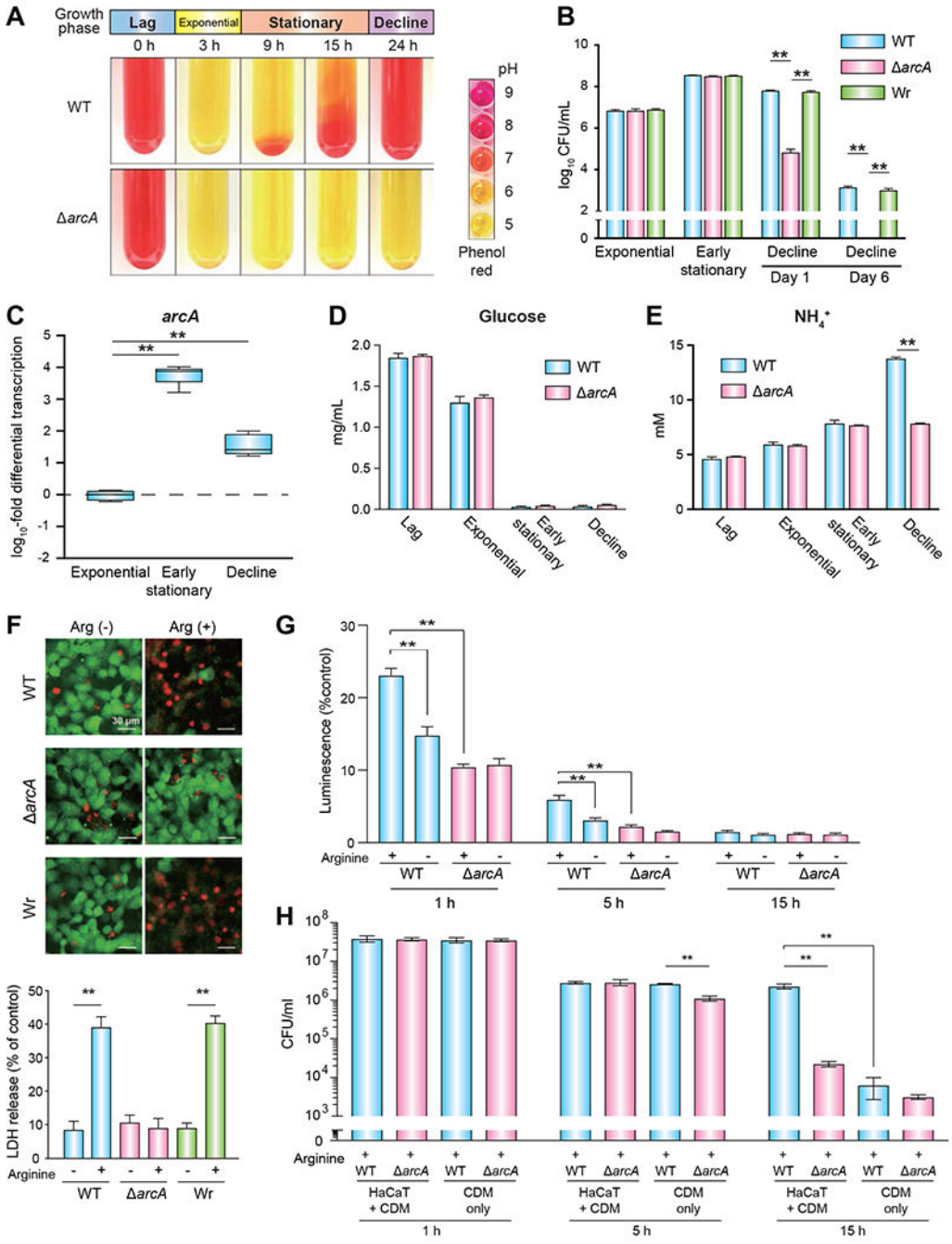

Figure 1. The *arcA* upregulation under glucose starvation condition, and arginine catabolism-dependent viability and cytotoxicity.

(A) Temporal pH change of bacterial cultures using phenol red broth supplemented with 30 mM arginine. (B) Bacterial growth ability and viability in THY broth. Error bars indicated the mean + S.E (n = 4). Representative data obtained from at least 3 independent experiments are shown. (C) The *arcA* expression of *S. pyogenes* WT at each growth phase within THY broth. Data obtained by combining 3 independent experiments are displayed with a box-whisker plot (n = 9). (D) Glucose and (E) ammonium ion levels in culture supernatant of WT (n = 9) and Δ*arcA* (n = 4) during growth in THY broth. Error bars

indicated the mean + S.E. (F) Arginine-dependent cytotoxicity of *S. pyogenes*. HaCaT cells cultured in CDM were infected with *S. pyogenes* (MOI = 500) for 20 h. Viable cells and dead cells are indicated green and red, respectively. LDH, lactate dehydrogenase. Values are presented as the mean of 4 wells from one of 3 independent experiments. Error bars indicated the mean + S.E. (G) Intracellular ATP levels of *S. pyogenes*. Representative data obtained from at least 3 independent experiments are shown. Vertical lines represent the mean + S.E (n = 4). (H) Bacterial viability in only CDM or CDM with cultured HaCaT cells. Error bars indicated the mean + S.E (n = 4). Representative data obtained from at least 3 independent experiments are shown. $^{**}p < 0.01$.

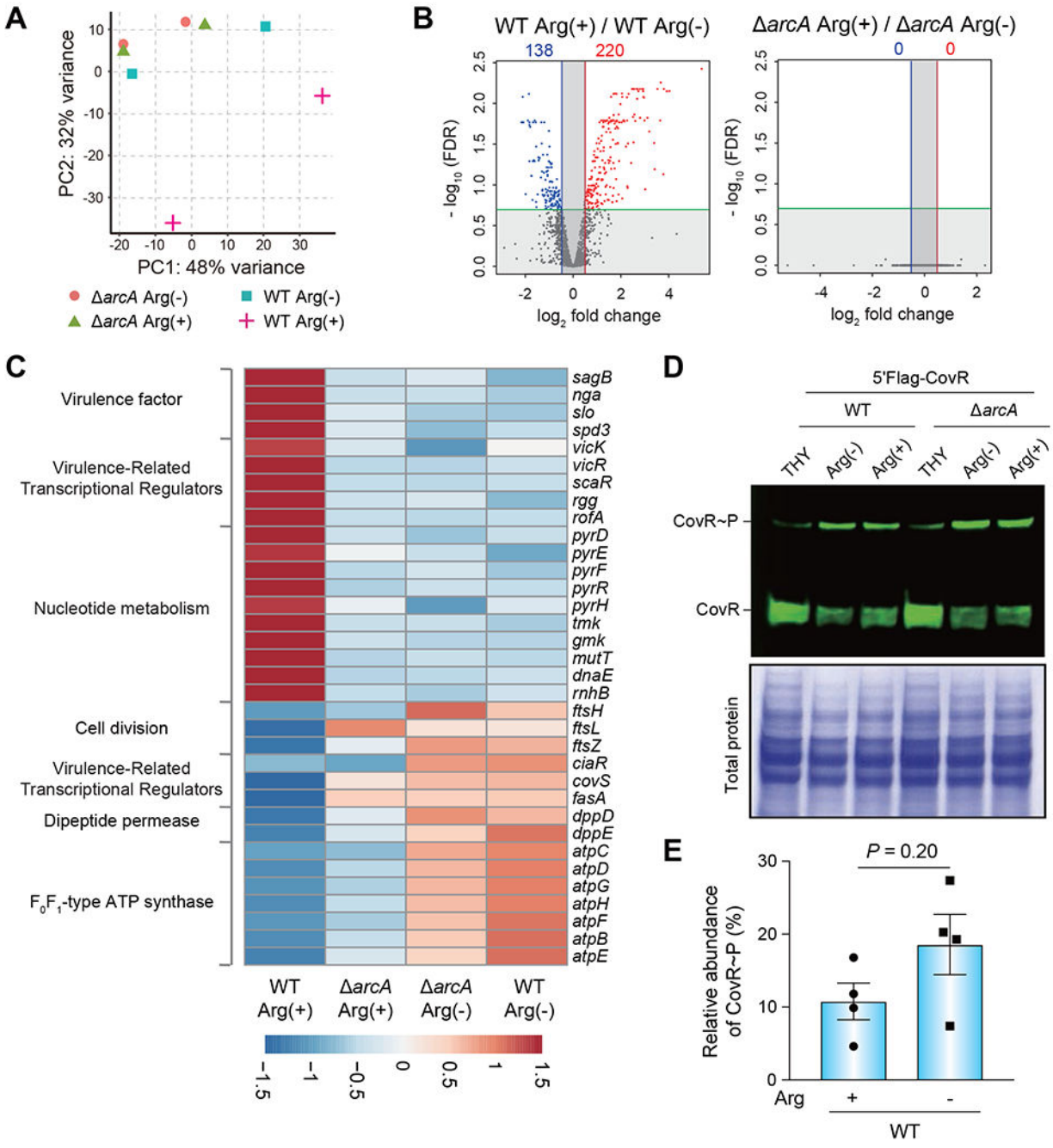

Figure 2. Effect of *S. pyogenes* arginine catabolism on transcriptome and phosphorylation of CovR.

(A) Principal component analysis (PCA) plot of Fragments Per Kilobase of exon per Million mapped fragments (FPKM) data from RNA-seq data set. (B) Valcano plots comparing global gene expression patterns between WT Arg(−) and WT Arg(+), and between Δ*arcA* Arg(−) and Δ*arcA* Arg(+). Colored circles indicate significantly upregulated (red) and downregulated (blue) genes (absolute log2 fold change, > 0.5; adjusted P < 0.2). (C) Heat map of up-or down-regulated functions. FPKM values were used for the heatmap visualization. Red and blue indicates induced and repressed, respectively. (D)

Phosphorylation levels of CovR. CovR~P and CovR indicate phosphorylated CovR and non-phosphorylated CovR, respectively. Total protein serves as the loading control. THY, RNA samples from exponential phase of *S. pyogenes* in THY medium. (E) Relative percentage of phosphorylated CovR. Error bars indicated the mean ± S.E (n = 4). Arg(−), strains in CDM without arginine. Arg(+), strains in CDM with 1000 μM arginine.

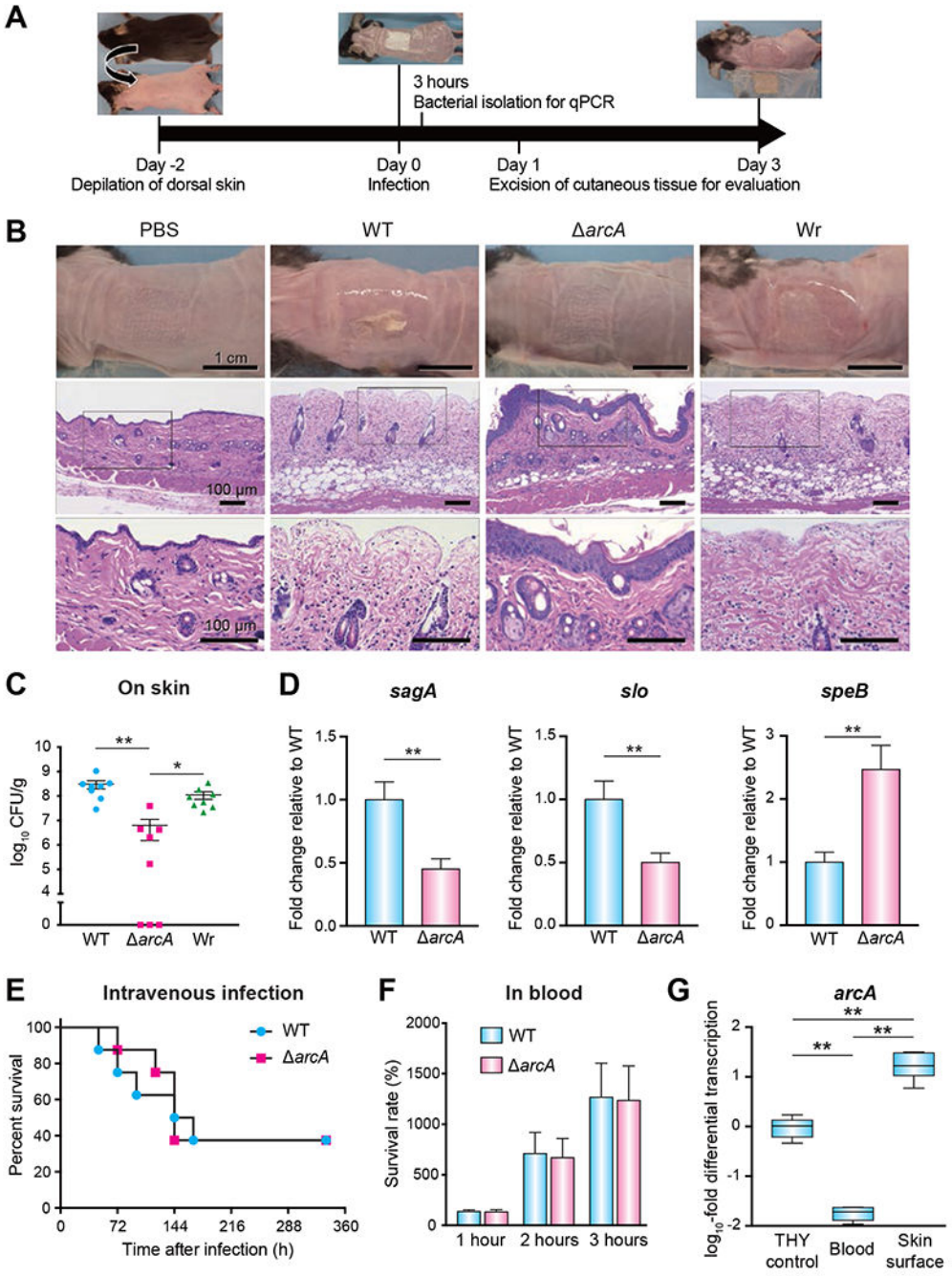

Figure 3. The roles of arginine catabolism for the virulence of *S. pyogenes* on the skin surface and in blood.

(A) Murine model of epicutaneous infection and its timeline. Mice were epicutaneously infected with 2×10^6 CFU of *S. pyogenes*. (B) Skin phenotype and histopathology at 3 days post-infection. Cutaneous tissues from infection sites were stained with HE. Data shown are representative of at least three separate experiments. (C) CFUs in skin lesions at 3 days post-infection. Data shown represent the mean ± S.E. (n = 8) and are representative of at least three independent experiments. (D) Expression levels of bacterial virulence genes, *sagA*, *slo*, and *speB*, on the skin surface. The *sagA, slo*, and *speB* gene expression levels in the Δ*arcA*

were examined by qPCR, and shown relative to that of the WT strain. The *16S rRNA* was used as the internal control. Data from three independent qRT-PCR assays, each performed in triplicate, were pooled and normalized. Vertical lines represent the mean + S.E. (E) Mouse model of intravenous infections. Mice were intravenously infected with 2×10^6 CFU of *S. pyogenes* (n = 8). Data are representative of at least three independent experiments. (F) Bacterial survival in mouse blood. Bacteria were incubated in heparinized mouse blood at 37°C for 1, 2, or 3 hours in a 5% CO_2 atmosphere. Survival rate was calculated by dividing the CFU value after the period of incubation by the CFU value of the original inoculum. Values are presented as the mean of 6 wells from one of 3 independent experiments. Vertical lines represent the mean + S.E. (G) The *arcA* expression of *S. pyogenes* WT in blood and on the skin surface. Data obtained by combining 3 independent experiments are displayed with a box-whisker plot (n = 9). THY control, RNA samples from exponential phase of *S. pyogenes* in THY medium. $^{**}p < 0.01$. $^{*}p < 0.05$.

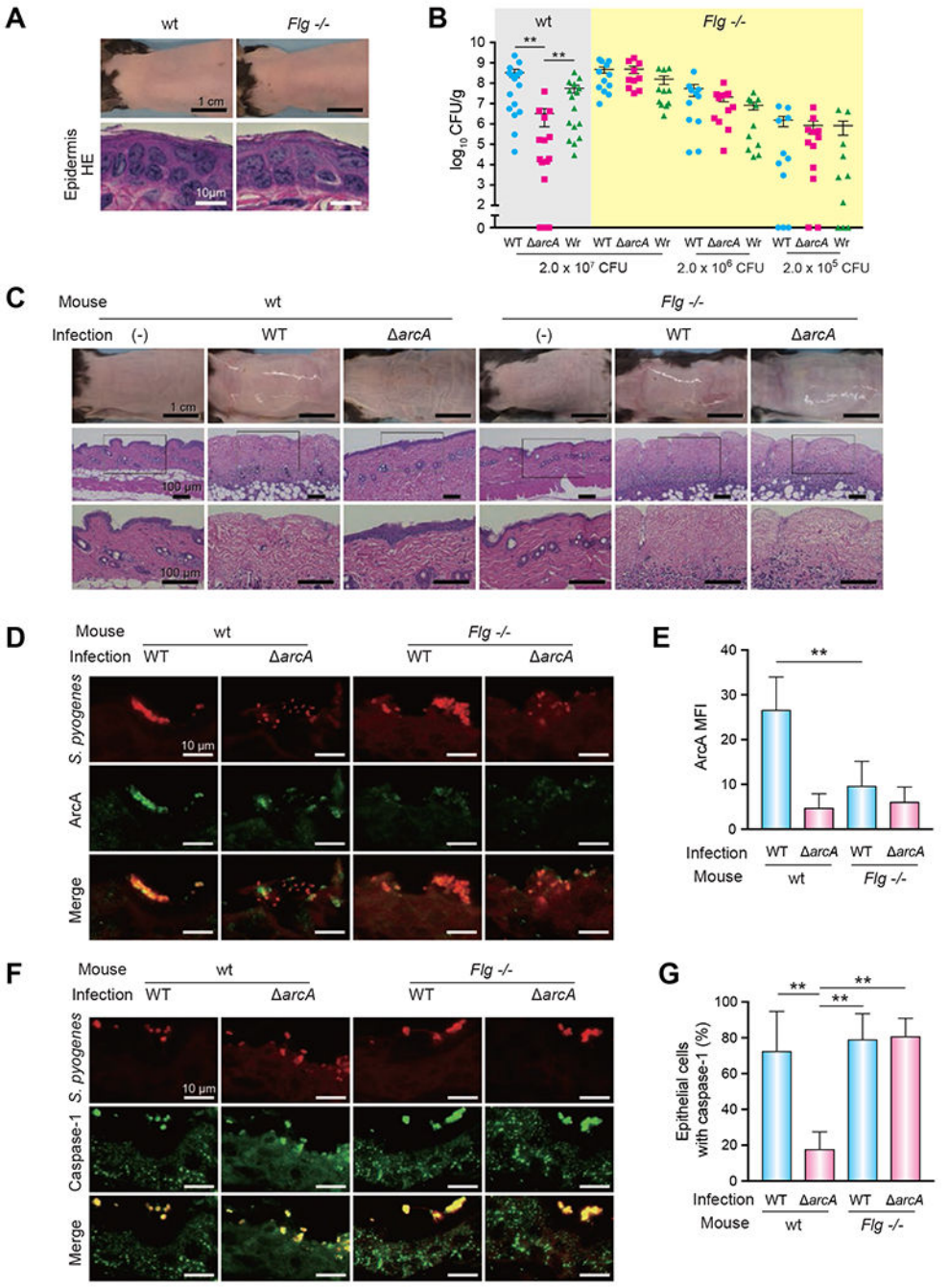

Figure 4. Arginine catabolism-independent virulence of *S. pyogenes* on the skin surface of filaggrin knock-out mice.

(A) Skin phenotype and histology both wt mice and *Flg*$^{-/-}$ mice. (B) CFUs in skin lesions at 3 days post-infection. Data shown represent the mean ± S.E. (n = 10-12). (C) Skin phenotype and histopathology at 3 days post-infection. Mice were epicutaneously infected with 2×10^7 CFU of *S. pyogenes*. Cutaneous tissues from infection sites were stained with HE. Data shown are representative of at least three separate experiments. (D) Representative microscopic images of immunofluorescence staining of *S. pyogenes* (red) and arginine deiminase, ArcA (green) on the skin surface at 24 hours post-infection. Strong merge signals

(yellow) were only detected in *S. pyogenes* WT on the skin surface of wt mice. (E) Mean fluorescence intensity (MFI) of ArcA (minimum 10 bacteria per condition, n = 8). MFI was quantified using ImageJ. Average background fluorescence was subtracted from each value. Data represent mean + S.E. (F) Representative microscopic images of immunofluorescence staining of *S. pyogenes* (red) on the skin surface and caspase-1 (green) in epidermis at 24 hours post-infection. Weak signals of epithelial cells were only shown in Δ*arcA*-infected wt mice. (G) The percentage of caspase-1 positive cells in epidermis (minimum 20 cells per condition, n = 8). Data represent mean + S.E. $^{**}p < 0.01$. $Flg^{-/-}$, filaggrin knock-out mouse, wt, wild-type mouse.

KEY RESOURCES TABLE

REAGENT or RESOURCE	SOURCE	IDENTIFIER
Antibodies		
Donkey anti-Goat IgG Alexa Fluor 594	Thermo Fisher Scientific	Cat# A32758
Donkey anti-Rabbit IgG H&L Alexa Fluor 488	Abcam	Cat# ab150065
Goat polyclonal anti-S. pyogenes carbohydrate	Abcam	Cat# ab9191
Rabbit polyclonal anti-caspase-1	GeneTex	Cat# GTX14368
Bacterial and Virus Strains		
Streptococcus pyogenes M1T1 strain 5448	Kansal et al., 2000	Accession:CP008776
XL-10 Gold	Agilent Technologies	Cat# 200314
Chemicals, Peptides, and Recombinant Proteins		
Carboxyfluorescein diacetate succinimidyl ester	Invitrogen	Cat# C1157
Mutanolysin	Sigma Aldrich	Cat# M9901
Staurosporine	Sigma Aldrich	Cat# S6942
Streptozotocin	Adipogen	Cat# 50-464-382
Critical Commercial Assays		
ATP-bioluminescent assay Kinshiro	TOYO B-Net	Cat# LL100-1
Click-iT Plus TUNEL Assay Kit (Alexa Fluor 488)	Thermo Fisher Scientific	Cat# C10617
Glucose Colorimetric Assay Kit II	Biovision	Cat# K686
LIVE/DEAD Viability/Cytotoxicity Kit	Thermo Fisher Scientific	Cat# L3224
Deposited Data		
Raw data files for RNA-sequencing	DDBJ SRA	DRA009112
Experimental Models: Cell Lines		
HEK-Blue IL-1β reporter cells	InvivoGen	Cat# hkb-il1bv2
Human: HaCaT cells	Boukamp et al., 1988	Human: HaCaT cells
Experimental Models: Organisms/Strains		
Filaggrin-null mouse strain (B6.Cg-Flg<tm1>)	RIKEN BRC	RBRC05850
Oligonucleotides		
See Table S2		
Recombinant DNA		
Plasmid: pSET4-ArcAKO	This paper	N/A
Plasmid: pSET4-5'Flag-CovR	This paper	N/A
Plasmid: pQE30_arcA	This paper	N/A
Software and Algorithms		
CLC Genomics workbench v. 9.5.2	Software	https://digitalinsights.qiagen.com/ja/qiagen-clc-genomics-workbench/

REAGENT or RESOURCE	SOURCE	IDENTIFIER
ClustVis	Software	https://biit.cs.ut.ee/clustvis/
GraphPad Prism7	Software	https://www.graphpad.com/scientific-software/prism/
iDEP.91	Software	http://bioinformatics.sdstate.edu/idep/
ImageJ	Software	https://imagej.nih.gov/ij/
ImageQuant software	Software	https://www.cytivalifesciences.com/en/us/shop/protein-analysis/molecular-imaging-for-proteins/imaging-software/imagequant-tl-8-1-p-00110
Other		
AimStrip Plus blood glucose meter kit	Germaine Labs	Cat# 37355
Citrate buffer	Bioworld	Cat# 40320056-2
cOmplete, EDTA (+) Protease Inhibitor Cocktail	Roche Molecular Diagnostic	Cat# 11697498001
Lysing Matrix B	Qbiogene	Cat# FAS-210
lysing Matrix D	Qbiogene	Cat# FAS-220
Nunc Lab-Tek II Chamber Slide System	Thermo Fisher Scientific	Cat# 154534
Phenol red broth	Sigma Aldrich	Cat# P8976
Phos-tag SuperSep™ Phos-tag™ Gels	Wako Pure Chemical Industries	Cat# 195-17991
PhosSTOP™	Roche Molecular Diagnostic	Cat# 4906845001
Quanti-Blue reagent	Invivogen	Cat# rep-qbs
RNAprotect Animal Blood Tubes	Qiagen	Cat# 76544
RNAprotect Bacteria Reagent	Qiagen	Cat# 76506
RNeasy Mini Kit	Qiagen	Cat# 74104
rRNA removal using a Ribo-Zero rRNA removal kit	Illumina Inc	Cat# 20040525
Superscript VILO cDNA synthesis kit	Thermo Fisher Scientific	Cat# 11756050
SYBR green RT-PCR master mix kit	Toyobo	Cat# QPK-201
Todd-Hewitt broth	BD Biosciences	Cat# 249240
TruSeq RNA Sample Prep kit, v2	Illumina Inc	Cat# RS-122
Yeast extract	BD Biosciences	Cat# 212750